A finite-difference time-domain solution to scattering from a rough pressure-release surface

Abbreviated title: FDTD method for rough surface scattering

Frank D. Hastings, email: fhasting@eecs.wsu.edu
John B. Schneider, email: schneidj@eecs.wsu.edu
Shira L. Broschat, email: shira@eecs.wsu.edu
School of Electrical Engineering and Computer Science
Washington State University
Pullman, WA 99164-2752
(509) 335-4655, FAX (509) 335-3818

Received:

Abstract

The finite-difference time-domain (FDTD) method is a numerical technique that makes no explicit physical approximations to the underlying problem. The quality of an FDTD-based solution typically is determined by the discretization of the computational domain—the smaller the spacing, the more accurate the solution. Unfortunately, for large computational domains, i.e., ones spanning many wavelengths, the small spatial step size needed to obtain a high-fidelity solution may lead to a prohibitively large number of unknowns. Here it is shown how the FDTD method can be used to model accurately scattering from pressure-release surfaces above a homogeneous water column. To keep the computational cost manageable, a number of enhancements to the standard FDTD algorithm are employed. These enhancements include correcting for numerical dispersion along the specular direction of the incident insonification, using locally conformal cells at the pressure-release boundary, and propagating the field through the homogeneous water column via an analytic method. The accuracy of the FDTD approach is demonstrated by comparison with an integral equation-based reference solution to the same rough surface scattering problem [Thorsos, *Proceedings of the Reverberation and Scattering Workshop*, 3.2-3.20 (1994)].

PACS numbers: 43.30.Gv, 43.30.Hw, 43.20.Fn

Introduction

The finite-difference time-domain (FDTD) method is a numerical technique that has been used to solve a wide range of problems for electromagnetic, acoustic, and elastic wave propagation (see, for example, [1, 2, 3]). While the FDTD method does not use any explicit physical approximations to the underlying problem, implicit approximations are inherent to any numerical method. For the FDTD method, these approximations include homogeneity of the material over individual cells and a "staircase" approximation to the interface between materials. One strength of a numerical method is that errors introduced by these implicit approximations can, in theory, be made vanishingly small. However, there is a trade-off between accuracy and computational cost. To obtain an accurate solution to a large problem using standard FDTD techniques, the number of unknowns required may be prohibitively large.

In this paper, it is shown that the FDTD method can be used to predict accurately the fields scattered from one-dimensional rough pressure-release surfaces spanning 200, or more, wavelengths of the insonification. This problem naturally lends itself to the use of several algorithm enhancements that permit an accurate solution at a reasonable cost and hence that make the solving of large problems feasible.

In a previous paper, the FDTD method was used in a Monte-Carlo technique to obtain scattering cross sections for randomly rough surfaces satisfying the Dirichlet boundary condition [4]. Both single-scale Gaussian and multiscale Pierson-Moskowitz surface roughness spectra were considered. The FDTD results agreed with those obtained by Thorsos using an integral equation (IE) technique [5]. However, the calculation of a scattering cross section, or scattering strength, requires the determination of fields far from the scatterer. Also, Monte

Carlo studies, such as the ones used in [4] and [5], require averaging of results over many surface realizations. Since near fields are typically more complicated than far fields and since averaging may mask small errors, it is possible that the FDTD method might not provide accurate results in the near-field for any single surface realization. To address this concern, this paper examines FDTD-based results for a reference problem for which an accurate IE-based solution exists [6]. For this problem, near field pressures are obtained for a single surface realization. Excellent agreement between the two solutions is obtained. Stephen has published an FDTD solution to the same problem, and his results agree well with the reference solution [7]. The work presented here differs from Stephen's in that the number of unknowns and the computational time are reduced by more than an order of magnitude. In addition, greater accuracy is obtained.

The FDTD method can be used to yield a full wave, time-domain solution to the surface scattering problem without placing restrictions on the underlying physical geometry. This allows the direct study of the scattering physics, but also permits benchmarking of approximate methods such as the small slope [8] and parabolic equation approximations [9]. Additionally, exact methods can be used to benchmark other less computationally expensive numerical methods. The reference problem considered here is a rigorous test of numerical accuracy; by comparing results in the near field, it is possible to detect small discrepancies that might not be evident in a far-field comparison. The results presented in this paper, in conjunction with those presented in [4], verify the accuracy of the FDTD method for the Dirichlet rough surface scattering problem.

The FDTD method is a time-domain method that can provide results over a broad frequency spectrum by means of a single simulation. However, since the reference problem and the corresponding IE reference solution were posed in the frequency domain, the FDTD solution presented here is restricted to a single frequency. Thus, we demonstrate the accuracy of the FDTD method, but do not concentrate on exploiting its full power.

In the next section, we describe the reference problem and present a comparison of the FDTD and IE results. In section 2 we discuss the details of implementing the FDTD method and the enhancements employed.

1 Reference Problem and Solution

The reference problem considered, Fig. 1, consists of a one-dimensional, rough pressure-release sea surface, an isovelocity water column, and harmonic tapered-beam insonification [6]. The rough surface is a single realization from a set of surfaces generated using a Pierson-Moscowitz wave number spectrum for a wind speed of 15 m/s [10]. The surface height is specified over a range of 750 m. The incident harmonic pressure is given at zero range, $x = 0$, by

$$p_{\text{inc}}(x=0,z) = \exp\left(-\frac{(z-z_0)^2}{g^2}\right)\exp\left(ikz\sin\theta_i\right) \tag{1}$$

where $\theta_i = 10°$ is the mean grazing angle, $g = 27.55$ m is the half power width, $z_0 = -66.12$ m is the location of the pressure maximum, and $k = 2\pi f/c$ m^{-1} is the wave number. The frequency f is 400 Hz and the sound speed in water c is 1500 m/s. Depth increases in the negative z direction. The FDTD simulation requires that the incident field be specified on the surface and also at the receiver. Using Green's second theorem, one can express the incident field at any point in the water column in terms of the field at zero range,

$$p_{\text{inc}}(x,z) = 2\int_{-\infty}^{\infty} p_{\text{inc}}(x'=0,z')\left.\frac{\partial G_0(x,z;x',z')}{\partial x'}\right|_{x'=0} dz' \tag{2}$$

where $G_0(x, z; x', z')$ is the two-dimensional free-space Green's function given by

$$G_0(x, z; x'z') = \frac{i}{4} H_0^{(1)} \left(k\sqrt{(x-x')^2 + (z-z')^2} \right) \tag{3}$$

The maximum value of $p_{\rm inc}(x=0, z)$ is unity and occurs at a depth of $z = z_0$. As written, (2), with the upper limit of integration at infinity, is for an infinite water column and is not directly applicable to the problem at hand. However, $p_{\rm inc}(x=0, z)$ is small for $z \geq 0$ m, so the integration can be truncated at an upper limit of zero without introducing significant error.

The goal of the reference problem is to find the total pressure at a range of 750 m over a 200 m depth starting at the surface (i.e., $x = 750$ m and $-200 \leq z \leq 0$ m). The reference solution was obtained using an IE technique [6]. Careful analysis was done to ensure that numerical errors were small.

Figure 2 shows a plot of the magnitude of the pressure over the 200 m depth for the reference solution and the FDTD solution. The two curves are nearly identical except near depths of 10 and 160 m, where there are slight differences. Adjusting the location of the absorbing boundary condition relative to the surface affected the error at 10 m. Hence, the discrepancy at this location is attributed to artifacts introduced by the absorbing boundary condition. This is discussed further in section 2.6. No obvious explanation was found for the discrepancy in the data at 160 m; it is most likely due to the differences between the FDTD and IE implementations. (For example, for the FDTD solution the elevation of the pressure-release surface was sampled every one-sixteenth of a wavelength, whereas for the IE solution the surface was sampled every one-tenth of a wavelength.) It should be noted that these differences and the resulting discrepancies in the data are well within practical limits.

Figure 3 shows the phase of the pressure for the reference solution and the FDTD solution.

(The branch cut was taken at 180 degrees and, for the sake of clarity, the segments are not connected across the cut.) Again, the reference solution and FDTD solution exhibit excellent agreement except near a depth of 10 m. The difference seen in the magnitude at 160 m is not present in the phase.

2 FDTD Implementation

2.1 Basic Equations

The governing acoustic equations in two dimensions are

$$\frac{\partial p}{\partial t} = -\rho c^2 \left(\frac{\partial v_x}{\partial x} + \frac{\partial v_z}{\partial z} \right) \tag{4}$$

$$\frac{\partial v_x}{\partial t} = -\frac{1}{\rho} \frac{\partial p}{\partial x} \tag{5}$$

$$\frac{\partial v_z}{\partial t} = -\frac{1}{\rho} \frac{\partial p}{\partial z} \tag{6}$$

where p is pressure, $\vec{v} = v_x \hat{\mathbf{a}}_x + v_z \hat{\mathbf{a}}_z$ is velocity, and ρ is density. For the reference problem the isovelocity water column has a density of 1000 kg/m^3. The update equations for the FDTD method are obtained by replacing the derivatives in (4)-(6) by finite differences and solving for "future" fields in terms of present and past fields. To obtain a fully explicit scheme the points at which the fields are evaluated must be offset spatially and temporally. Second-order accurate central differences can be used to approximate all the derivatives if the fields are discretized so they are defined at the following evaluation points:

$$p(x, z, t) = p(i\Delta x, j\Delta z, n\Delta t) = p^n(i, j) \tag{7}$$

$$v_x(x, z, t) = v_x\left((i + 1/2)\Delta x, j\Delta z, (n + 1/2)\Delta t\right) = v_x^{n+1/2}(i, j) \tag{8}$$

$$v_z(x, z, t) = v_z\left(i\Delta x, (j + 1/2)\Delta z, (n + 1/2)\Delta t\right) = v_z^{n+1/2}(i, j) \tag{9}$$

where Δx and Δz are the range and depth spatial step sizes, respectively, and Δt is the temporal step size. A portion of the FDTD grid is shown in Fig. 4. In this work $\Delta x = \Delta z = \delta$. On the right-hand side of (7)-(9), the fields are specified by their spatial and temporal indices, i.e., the arguments and the superscripts, respectively. For the v_x and v_z components of velocity, the spatial offsets are implied by the field component (i.e., $v_x(i,j)$ is not collocated with $v_z(i,j)$). The temporal offset between the fields is explicitly retained in the temporal index. Replacing the derivatives in (4)-(6) with finite differences and using the discretization of (7)-(9) yields the following update equations:

$$\begin{aligned} p^n(i,j) &= p^{n-1}(i,j) - \rho c \frac{c\Delta t}{\delta}\Big[v_x^{n-1/2}(i,j) - v_x^{n-1/2}(i-1,j) + \\ &\qquad v_z^{n-1/2}(i,j) - v_z^{n-1/2}(i,j-1)\Big] && (10) \\ v_x^{n+1/2}(i,j) &= v_x^{n-1/2}(i,j) - \frac{1}{\rho c}\frac{c\Delta t}{\delta}\left[p^n(i+1,j) - p^n(i,j)\right] && (11) \\ v_z^{n+1/2}(i,j) &= v_x^{n-1/2}(i,j) - \frac{1}{\rho c}\frac{c\Delta t}{\delta}\left[p^n(i,j+1) - p^n(i,j)\right] && (12) \end{aligned}$$

These equations are used in a leap-frog scheme to obtain the unknown future fields in terms of the known past and current fields. This explicit scheme, unlike many implicit schemes, is not unconditionally stable. To obtain a stable solution in two dimensions, the factor $c\Delta t/\delta$, known as the Courant number, must be less than or equal to $1/\sqrt{2}$. (For more information on the Courant number and stability of the FDTD method the reader is referred to [1].)

The remainder of this paper discusses the application of these equations to solving the reference problem. Several enhancements that are not found in "traditional" FDTD-based solutions are presented. Collectively, these enhancements enable the FDTD method to produce accurate results at a reasonable computational cost.

2.2 Incident Field and Scattered-Field Formulation

Insonification of the FDTD grid was accomplished using a scattered-field approach for which the field at the pressure-release surface is set to the negative of the incident field. Hence, it was necessary to calculate the incident field at the surface. Incident field data were available from Thorsos in a format suitable for the IE method [6]. However, since the elevations of the pressure-release surface were sampled at different ranges for the FDTD solution, it was necessary to use an independent calculation of the incident field. For the IE solution, (2) was integrated using a single-precision, Riemann sum over the limits -150 m $\leq z \leq 0$ m. For the FDTD solution, a semi-infinite, double-precision integral was used. Integration was performed with an adaptive quadrature routine from the QUADPACK integration package [11].

To exploit fully the power of the FDTD technique, the incident insonification should be transient, allowing information to be obtained over a band of frequencies. However, when results are needed for only a single frequency, as for the case here, one can either use transient insonification and extract the information at the desired frequency or, alternatively, use "quasi-harmonic" illumination and wait for the transients to die out. By "quasi-harmonic" we mean the excitation is zero at the start of the simulation but then, after a gradual ramp in magnitude as described below, varies harmonically. Each approach requires approximately the same number of time steps. With the first approach, the simulation must be run until all energy has propagated out of the computational domain to prevent frequency aliasing. With the second approach, the simulation must be run until all transients dissipate and steady state is obtained. Since the reference problem specified the insonification at a single frequency and a suitable analytic expression for transient illumination was not readily available, we used a quasi-harmonic incident field.

For a point (x_s, z_s) on the surface, (2) can be used to obtain the scattered field phasor $A_s \exp(-i\alpha_s)$ (the scattered field is the negative of the incident field as reflected in the phase of α_s). In the time domain this becomes $A_s \cos(\omega t + \alpha_s)$. Use of this time-domain representation for all surface points throughout the computational domain would cause an exceedingly large transient since all the surface fields would switch on simultaneously. An excessive number of time steps would then be required to dissipate this transient. The transient associated with the introduction of the incident field can be reduced significantly by gradually turning on the field. This can be accomplished by weighting the amplitude of the surface fields in accordance with a temporally ramped plane wave. Specifically, for points on the surface the scattered pressure is

$$p_s(x_s, z_s, t) = A_s \cos(\omega t + \alpha_s) u(\xi) \left[1 - \exp\left(-\xi^2/\tau^2\right)\right] \tag{13}$$

where $\xi = ct - x_s \cos\theta_i - z_s \sin\theta_i$, u is the unit step function, and θ_i is the incident angle. The time constant τ controls the rate at which the surface fields ramp up to their final values; for this work, it was set to approximately ten periods of the harmonic insonification. This modified form of the incident field affects only the transient and not the steady-state behavior.

2.3 Near-Field to Near-Field Transformation

As shown in Fig. 1, the reference problem requires calculation of the scattered field over a 200 m depth at a range of 750 m, i.e., over the line labeled "receiver." An FDTD grid can be constructed to span the entire receiver. After steady state has been obtained, the scattered field at the receiver is then recorded directly from the grid. However, this is not the most efficient approach. Since the water column is homogeneous, it is possible to calculate analytically the scattered field at any point in the water column using a near-field to near-field (NFNF) transformation. This approach has two important advantages over a direct FDTD solution: (1) the computational domain is much smaller and (2) the effects of numerical dispersion are reduced. As a result, the computational cost is reduced while, at the same time, the accuracy is improved.

Implementation of the NFNF transformation is straightforward. Once steady state is reached, the scattered fields are recorded over an imaginary boundary three cells below the lowest point of the surface. This boundary is referred to as the data collection zone and is shown in Fig. 5. Again employing an analytic expression, similar to (2), the scattered fields at the "receiver" are calculated from the measured fields.

Steady state was defined to exist when the magnitudes and phases no longer changed significantly from one period of the incident field to the next. The simulation was terminated when the average relative change in magnitudes was less than 0.001 and the average change in phase was less than 0.05 degrees. To obtain the values of the magnitudes and phases, the required fields were sampled twice each period along the data collection zone. With harmonic oscillation assumed, the two samples were sufficient to determine the magnitude and phase of the signal.

In the NFNF approach, the computational domain is made large enough to accommodate the surface, the data collection zone, and the absorbing boundary condition. In comparison with the standard FDTD approach, for which the computational domain encloses the entire receiver, the vertical dimension of the domain is reduced by approximately 91%. In addition, for the NFNF approach the fields propagate only from the surface to the data collection zone before they are measured, in contrast to the standard FDTD approach for which the fields propagate from the "transmitter" to the "receiver." The error introduced by numerical dispersion increases with the distance the fields propagate. Hence, this error is significantly smaller for the NFNF approach as discussed further in the next section.

2.4 Dispersion Correction

Equations (10)-(12) are inherently dispersive. For a plane wave propagating in the FDTD grid at an angle ϕ with respect to the x axis, the numeric dispersion relation is

$$\left(\frac{\delta}{c\Delta t}\right)^2 \sin^2\left(\frac{\omega\Delta t}{2}\right) = \sin^2\left(\frac{\delta\tilde{k}\cos\phi}{2}\right) + \sin^2\left(\frac{\delta\tilde{k}\sin\phi}{2}\right) \tag{14}$$

where $\tilde{k}$ is the wave number for the fields propagated by the FDTD simulation and ω is the frequency [1]. This reduces to the usual continuous-space dispersion relation, i.e., $k^2 = \omega^2/c^2$, in the limit as δ and Δt approach zero. (Note that the FDTD scheme used here discretizes the coupled first-order governing differential equations. However, the dispersion relation is the same for the discretized form of the wave equation [12].)

To minimize the memory required for a simulation, the coarsest possible grid should be used. However, in practice, certain errors increase as the spatial step size increases, thus imposing limits on the coarseness of the grid. These errors are associated with (1) assuming homogeneity for a material over discrete "cells," (2) approximating material boundaries as "staircased," and (3) numeric dispersion. In the problem under consideration, the water column is homogeneous so the first source of error is not relevant. The second source of error is considered in the next section. The error associated with numeric dispersion, i.e., the amount that $\tilde{k}$ differs from the true wave number, is a function of the spatial step size, the angle of propagation, and the Courant number. For a given spatial step size and propagation angle, the error is at a minimum at the Courant limit (which is $1/\sqrt{D}$ where D

is the number of spatial dimensions in the problem) [13, 14]. Thus, the Courant limit was used for the FDTD solution to the reference problem. A spatial step size of one-sixteenth of a wavelength is not uncommon in FDTD simulations involving objects (scatterers) less than 10 wavelengths in size. This discretization, though considered large, was found to be acceptable for the reference problem provided corrections were made for numeric dispersion as described below.

At 16 points per wavelength (PPW) and the Courant limit and assuming plane wave propagation at an angle of 10° (i.e., $\phi = 10^\circ$ in (14)), the phase velocity in the FDTD grid is 0.287% slower than the true phase velocity. This difference in velocity seemingly is small, but the error associated with it is cumulative. After a wave propagates through a large computational domain, such as the one considered here, the total phase error can be quite large. Here the difference between k and $\tilde{k}$ produces approximately one degree of phase error per wavelength of propagation. Thus, propagation across the entire 200-wavelength computational domain would result in 200 degrees of phase error.

As discussed in section 2.3, an NFNF transformation was used to obtain the fields at the receiver. By analytically "propagating" fields whenever possible, a much smaller computational domain was used than would otherwise have been required. However, this scheme mixes analytic and numeric wave numbers over a large computational domain, requiring that the two wave numbers agree more closely than they do using discretization of 16 PPW in the tradition FDTD method. Fortunately, this problem can be solved in one of two ways: (1) the analytic wave number can be increased to agree with the numeric one or (2) the material parameters in the simulation can be adjusted to make the numeric wave number agree with the analytic one. In this work, the former approach was used. Thus, in analytic expressions, k was replaced by $1.00288k$. Since the wavelength in the FDTD simulation was contracted, the height and length of the pressure-release surface were scaled correspondingly (divided by a factor of 1.00288). Finally, when transforming back into physical space from numeric space (points in the FDTD grid), the spatial coordinates were re-scaled by multiplying by a factor of 1.00288.

The reference problem is well suited to such a simple dispersion correction since the incident field propagates primarily in a single direction (i.e., although the incident insonification is not a plane wave, most of the incident energy propagates at an angle ϕ close to 10° grazing). If the incident field were not approximately planar (e.g., the field due to a line source near the surface), it would be difficult to define a meaningful dispersion correction factor, and dispersion errors would have to be controlled by a suitable selection of the PPW.

It should be noted that for the problem considered here, the benefits of using a dispersion correction are not restricted to results near the specular direction (10° grazing). The fields coupled into the grid are dictated by an analytic expression for the incident field. It is important that the phase velocity (or wave number) of the analytic expression and the phase velocity of the fields in the grid are matched. Without proper matching, the fields coupled into the grid will behave as if the incident field arrived at an angle other than the true incident angle. By correcting for numerical dispersion, the incident angle is true. However, the scattered fields do leave the surface at all angles. Thus, energy that is propagating in directions other than specular (or backscatter) will suffer some numerical dispersion since the dispersion correction is only exact for a single angle. However, these scattered fields are recorded (at the data collection zone) after traveling only a short distance and hence, at that point, have not accumulated any significant phase error. Since the fields are analytically propagated after being recorded, no additional phase error is ever introduced.

The type of dispersion correction described above is not restricted to the Dirchlet problem. It can be applied equally well to fluid-fluid and fluid-elastic interface problems.

2.5 Surface Realization and Conformal Cell

The reference problem specified heights to a high degree of accuracy, but only at discrete range samples separated by one-tenth of a wavelength. Since the FDTD simulation requires a finer discretization in range, it was necessary to interpolate between the surface heights provided. Hence, the resulting surface was slightly different than that used for the IE method.

A standard FDTD implementation uses a Cartesian grid that allows specification of media only to within a grid space. As a result, curved boundaries are modeled using a staircase approximation as shown in Fig. 4(a). Such an approximation can produce significant artifacts due to nonphysical scattering. This is remedied either by using a very finely discretized grid or by using a conformal technique for which the grid structure is altered to conform to the scatterer. In this work, a locally conformal technique was used based on the integral form of (5) and (6). Rewriting these equations as a single vector equation and taking the volume integral of both sides yields

$$\int_V \frac{\partial \vec{v}}{\partial t} dv = -\int_V \frac{1}{\rho} \nabla p dv \tag{15}$$

Using the identity $\int_v \nabla \phi dv = \int_s \phi \hat{n} ds$ and reducing to the 2D case yields

$$\int_S \frac{\partial v_x}{\partial t} ds = -\oint_l \frac{1}{\rho} p n_x dl \tag{16}$$

$$\int_S \frac{\partial v_z}{\partial t} ds = -\oint_l \frac{1}{\rho} p n_z dl \tag{17}$$

where surface S and contour l are shown in Fig. 4(b) and 4(c) for field components v_x and v_z, respectively. The quantities n_x and n_z are the x and z components, respectively, of the outward unit normal vector along the contour. This method is analogous to that introduced by Jurgens *et al.* [15]. It is assumed that v_x and v_z are constant over S and p is constant over each segment of the contour. To satisfy the Dirichlet boundary condition, the pressure on the surface is set to the negative of the incident field. The incident field is computed at the center of the contour segment adjoining the surface. Under these assumptions, (16) and (17) reduce to the time-stepping relations

$$v_x^{n+1/2}(i,j) = v_x^{n-1/2}(i,j) - \frac{\Delta t}{\frac{1}{2}(l_1+l_2)\delta\rho}(p^n(i,j) - \sqrt{1+(l_2-l_1)^2}\; n_x p_{\rm inc}) \tag{18}$$

$$v_z^{n+1/2}(i,j) = v_z^{n-1/2}(i,j) - \frac{\Delta t}{\frac{1}{2}(l_3+l_4)\delta\rho}(p^n(i,j+1) - \sqrt{1+(l_3-l_4)^2}\; n_z p_{\rm inc}) \tag{19}$$

where lengths l_1, l_2, l_3, and l_4 are shown in Fig. 4(b) and 4(c).

Pressure nodes that have one or more neighboring velocities above the pressure-release surface are not used. Instead, the velocities that would normally depend on them for update are computed using extended cells. Hence, no special update equation is needed for pressure nodes that occur near the surface. To obtain (18) and (19) the conformal cells are approximated as trapezoids. This introduces a slight change in the surface geometry; however, the difference is small compared to the staircase approximation. Conformal-cell updates only occur near the interface; in fact (16) and (17) reduce to (11) and (12) for square cells.

Many of the locally-conformal schemes developed for electromagnetics problems can be adapted for acoustics problems. The method used here is adapted from one developed for electromagnetic scattering from perfect electric conductors [15]. Fluid-fluid boundaries are analogous (in 2-D) to dielectric-dielectric boundaries and hence the locally-conformal schemes which have been developed for dielectric interfaces can be used to solve fluid-fluid problems. These methods are not restricted to surface scattering problems such as the one considered here—they can also be applied to discrete scatterers with complicated geometries including wedges, slots, and curved surfaces [1].

2.6 Absorbing Boundary Conditions

For unbounded problems, an FDTD simulation requires the use of absorbing boundary conditions (ABCs). Here, the perfectly matched layer (PML) [16] ABC was used. As shown in Fig. 5, the ABC bounds the computational domain below the surface and terminates on the edges at the water-air interface. The surface was extended with flat buffer zones on either end to accommodate the PML. The PML thickness used was 16 grid spaces.

A minimum vertical grid dimension of 78 cells was used to accommodate the surface and the PML. Increasing this value caused a change in the results at a depth of 10 m; however, the magnitude of the difference between the FDTD and reference solutions remained relatively constant. Hence, it is likely that reflections from the ABC were the cause of the discrepancy at the 10 m depth. To eliminate completely spurious energy from the ABC, it would be necessary to increase the size of the computational domain to such an extent that the problem would become numerically intractable. However, given the published literature documenting the excellent overall performance of the PML ABC and the weak dependence of the observed results on the size of the computational domain, one can be confident that the error introduced by the PML is small.

2.7 Comparison with Another FDTD Solution

An FDTD-based solution to the reference problem has been published by Stephen [7]. His solution is based on the full-grid implementation—that is, the computational domain fully encompasses the surface, "transmitter," and "receiver." The incident field is propagated directly from the "transmitter" via the FDTD grid, and no NFNF transformations are used. Table 1 lists some of the differences between the full-grid solution and the solution presented here. The full-grid solution agreed well with the reference solution. However, with the exception of the field near a depth of 10 m, the results presented in this paper agree better with the reference solution than do the full-grid results. The full-grid solution was obtained using 20 PPW instead of 16. The amount of phase error due to dispersion is reduced 36% by increasing the PPW from 16 to 20. However, the NFNF approach with the dispersion correction had better overall accuracy. From Table 1, it is apparent that the NFNF approach is computationally more efficient than the full-grid approach. However, the implementation used in [7] was a general elastic/acoustic scheme. The use of strictly acoustic update equations would reduce the number of unknowns and run time shown for the full-grid approach by a factor of approximately 3/5. The run times shown in Table 1 provide an estimate of the speed-up that can be realized using the approach presented here (which is more than an order of magnitude faster). However, although the machines on which these codes were run are roughly comparable in computational power, factors such as clock speed, cache size, and compiler optimization will also influence run times.

3 Summary

An FDTD method for simulating scattering from rough, pressure-release surfaces has been presented. The approach relies on a near-field to near-field transformation to reduce computational cost and utilizes a correction for the inherent numerical dispersion of the FDTD method. A conformal grid technique was used to model more accurately the surface geometry at a modest number of points per wavelength (16 PPW). An alternate full-grid FDTD implementation was compared with the NFNF implementation presented here. The comparison shows that the NFNF approach has better overall accuracy and is far more computationally efficient than the full-grid scheme. Finally, the FDTD solution was compared with the IE reference solution and results for both the magnitude and phase are virtually the same.

Acknowledgments

This work was supported by the Office of Naval Research, Code 321OA.

References

[1] A. Taflove, *Computational Electrodynamics: The Finite-Difference Time-Domain Method.* Boston, MA: Artech House, 1995.

[2] J. Virieux, "*P-SV* wave propagation in heterogeneous media: Velocity-stress finite difference method," *Geophysics*, vol. 51, no. 4, pp. 889–901, 1986.

[3] D. Botteldooren, "Acoustical finite-difference time-domain simulation in a quasi-Cartesian grid," *J. Acoust. Soc. Am.*, vol. 95, no. 5, pp. 2313–2319, 1994.

[4] F. D. Hastings, J. B. Schneider, and S. L. Broschat, "A Monte-Carlo FDTD technique for rough surface scattering," *IEEE Trans. Antennas Propagat.*, vol. 43, pp. 1183–1191, Nov. 1995.

[5] E. I. Thorsos, "The validity of the Kirchhoff approximation for rough surface scattering using a Gaussian roughness spectrum," *J. Acoust. Soc. Am.*, vol. 83, pp. 78–92, 1988.

[6] E. I. Thorsos, "Test Case 1: Sea surface forward scattering," in *Proceedings of the Reverberation and Scattering Workshop* (D. B. King, S. A. Chin-Bing, J. A. Davis, and R. B. Evans, eds.), (Gulfport, MS), pp. 3.2–3.20, May 1994. Naval Research Laboratory Book Contribution NRL/BE/7181-96-001.

[7] R. A. Stephen, "Modeling sea surface scattering by the time-domain finite-difference method," *J. Acoust. Soc. Am.*, vol. 100, no. 4, pp. 2070–2078, 1996.

[8] A. Voronovich, *Wave Scattering from Rough Surfaces.* Berlin: Springer-Verlag, 1994.

[9] F. B. Jensen, W. A. Kuperman, M. B. Porter, and H. Schmidt, eds., *Computational Ocean Acoustics.* New York: American Institute of Physics, 1994.

[10] E. I. Thorsos, "Acoustic scattering from a "Pierson-Moskowitz" sea surface," *J. Acoust. Soc. Am.*, vol. 88, pp. 335–349, 1990.

[11] R. Piessens, E. de Doncker, C. Uberhuber, and D. Kahaner, *QUADPACK, A Subroutine Package for Automatic Integration.* Berlin: Springer-Verlag, 1983.

[12] R. M. Alford, K. R. Kelly, and D. M. Boore, "Accuracy of finite-difference modeling of the acoustic wave equation," *Geophysics*, vol. 39, no. 6, pp. 834–842, 1974.

[13] A. C. Cangellaris and R. Lee, "On the accuracy of numerical wave simulations based on finite methods," *J. Electromagn. Waves Applicat.*, vol. 6, no. 12, pp. 1635–1653, 1992.

[14] K. L. Shlager, J. G. Maloney, S. L. Ray, and A. F. Peterson, "Relative accuracy of several finite-difference time-domain methods in two and three dimensions," *IEEE Trans. Antennas Propagat.*, vol. 41, pp. 1732–1737, Dec. 1993.

[15] T. G. Jurgens, A. Taflove, K. Umashankar, and T. G. Moore, "Finite-difference time-domain modeling of curved surfaces," *IEEE Trans. Antennas Propagat.*, vol. 40, pp. 357–366, Apr. 1992.

[16] J.-P. Berenger, "A perfectly matched layer for the absorption of electromagnetic waves," *J. Comput. Phys.*, vol. 114, no. 1, pp. 185–200, 1994.

	full-grid	NFNF
Points/λ:	20	16
Field:	Total	Scattered
Code type:	Elastic	Acoustic
Grid:	Stairstep	Conformal
Unknowns:	$\approx 27 \times 10^6$	$\approx 0.8 \times 10^6$
Time Steps:	7205	5400
Run Time:	9h 22min	38 min
Machine:	DEC Alpha 3000/400	HP 9000/735

Table 1: Resource comparison for full-grid and the near-field to near-field (NFNF) transformation implementations.

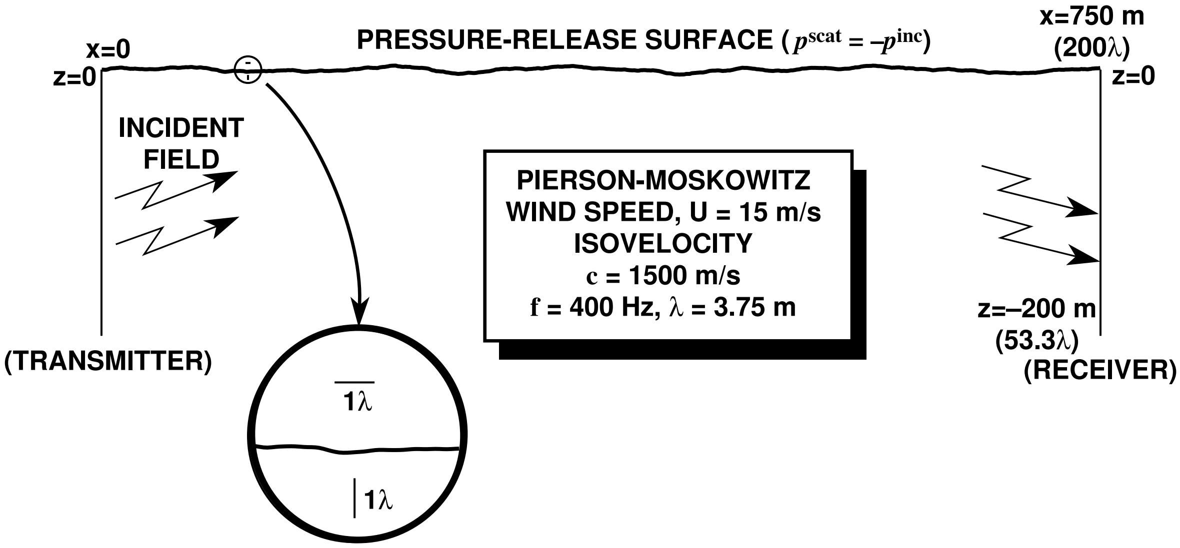

Figure 1: Reference problem geometry. The surface is drawn to scale. The expanded view shows a segment of the surface and lines with lengths equal to one wavelength of the insonification. The incident field is specified at a range of zero (identified as the transmitter). The goal is to determine the scattered pressure at a range of 750 m over a depth of 200 m (identified as the receiver). The terms transmitter and receiver are used logically and are not meant to imply the existence of a physical device at these locations.

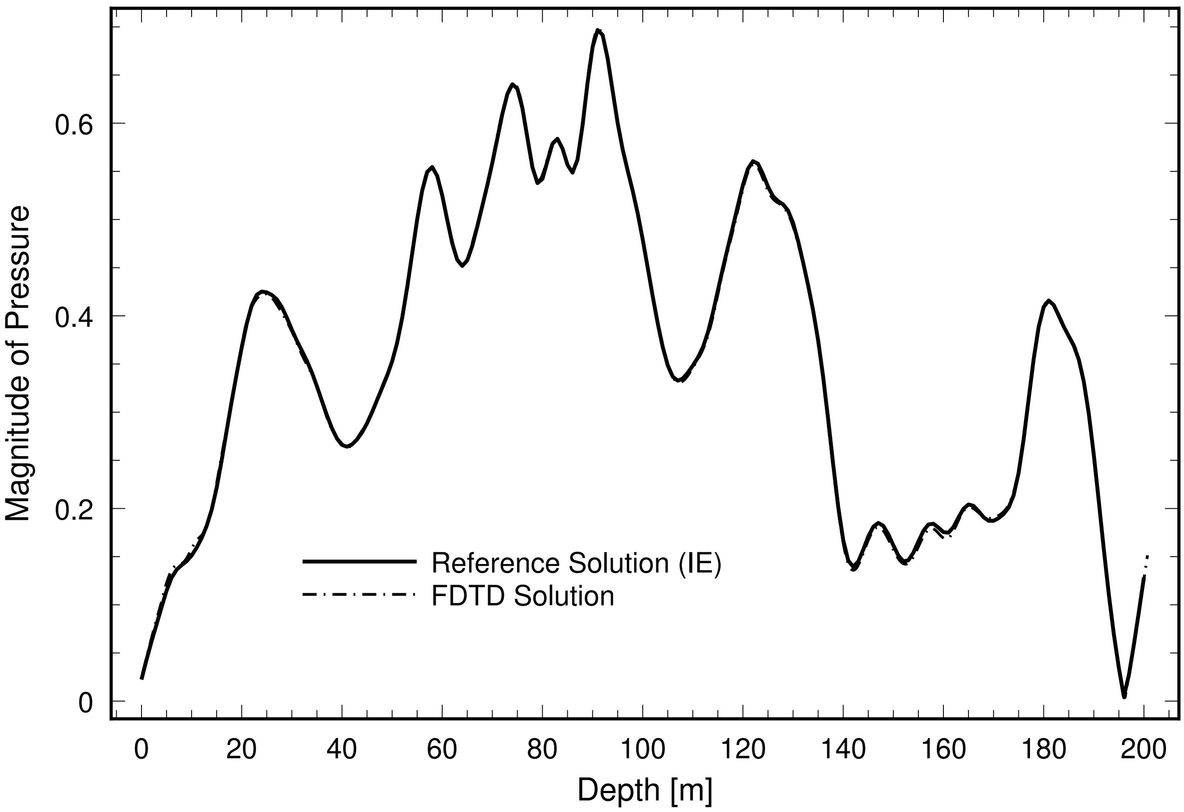

Figure 2: Pressure magnitude over a depth of 200 m at a range of 750 m. Reference solution and FDTD solution.

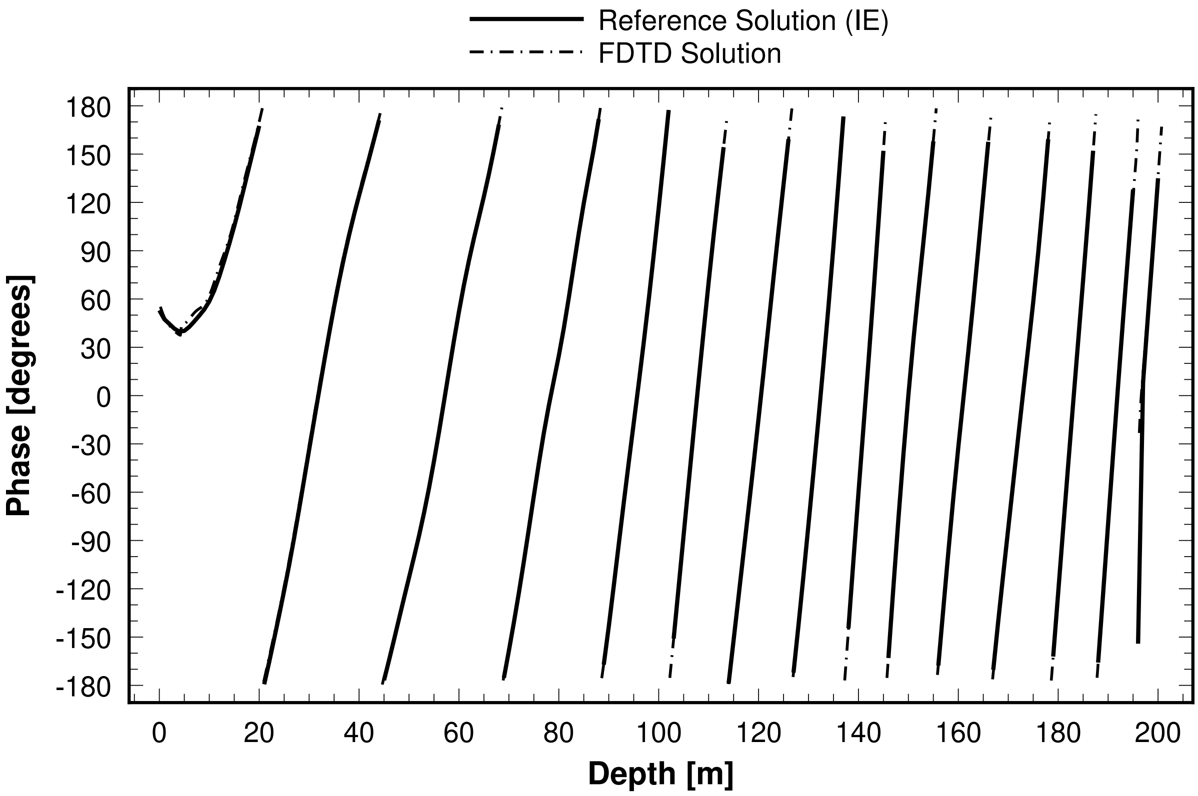

Figure 3: Pressure phase over a depth of 200 m at a range of 750 m. Reference solution and FDTD solution.

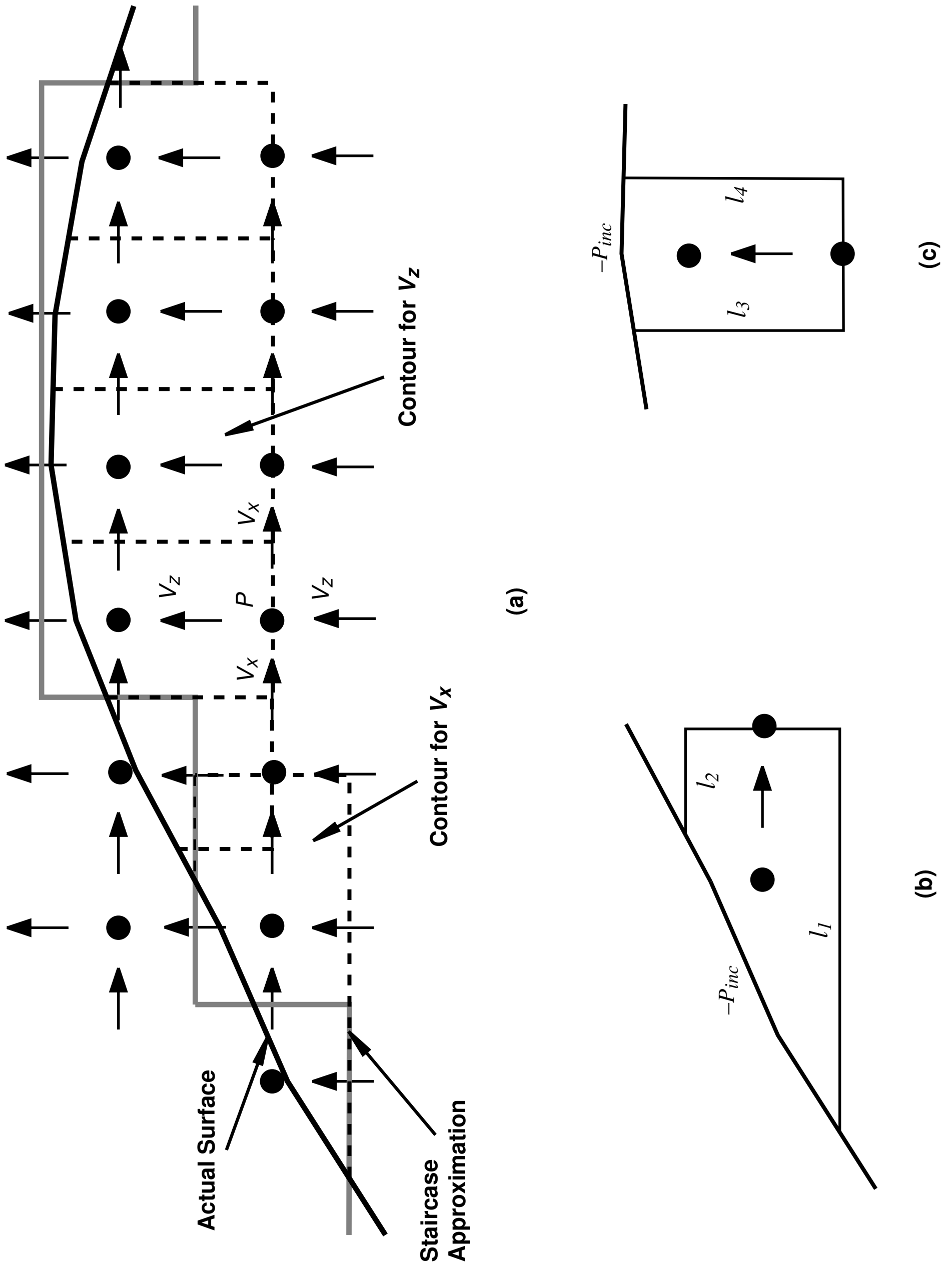

Figure 4: Staircase and contour path models of the surface are shown. Part (a) shows the actual surface (black solid line) with staircase approximation (grey solid line) and conformal cells (dashed lines). The conformal cells are bounded on the top by the actual surface. Conformal cells are shown for v_x and v_z in parts (b) and (c), respectively.

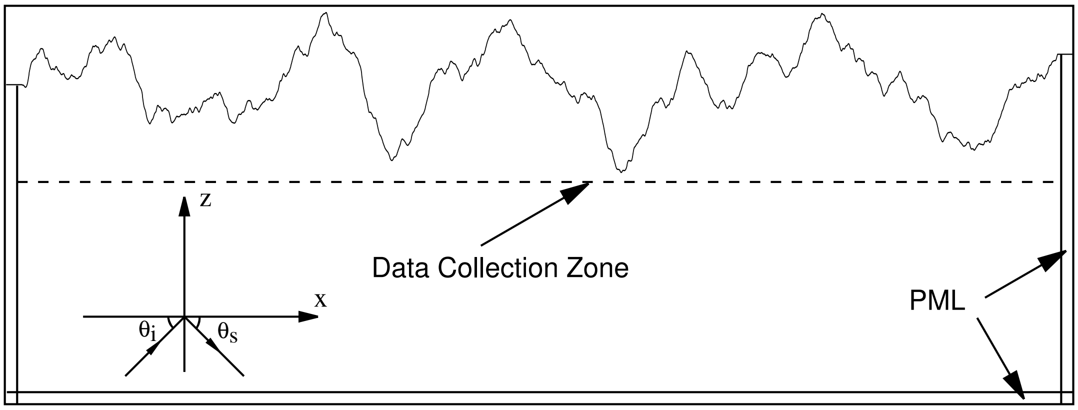

Figure 5: Computational domain for the FDTD simulation. The PML ABC bounds the lower edge and part of the sides of the domain. The measurement boundary is the line over which the pressures and velocities are measured for transformation to the "receiver." In this figure the vertical scale has been expanded by a factor of approximately 15.